Calibrating a fiber–matrix interface failure model to single fiber push-out tests and numerical simulations

Benedikt Rohrmüller [a,b,*], Peter Gumbsch [a,b], Jörg Hohe [b]

[a] *Institute for Applied Materials, Karlsruhe Institute of Technology (KIT), Straße am Forum 7, 76131 Karlsruhe, Germany*
[b] *Fraunhofer Institute for Mechanics of Materials IWM, Wöhlerstr. 11, 79108 Freiburg, Germany*

ARTICLE INFO

ABSTRACT

To characterize the fiber–matrix interface of a glass-fiber reinforced sheet molding compound (SMC), single-fiber push-out tests are performed and simulated numerically. The parameters of a cohesive zone model for the interface are calibrated on the single-fiber push-out tests. The fracture-toughness/energy release rate therein is determined from cyclic (loading–unloading) experiments. The matrix model, consisting of the nonlinear-elastic Neo-Hooke law with a Prony series to model viscoelastic behavior, is calibrated with data from nanoindentation tests by adjusting simulation curves to their experimental counterparts. Using the calibrated model of the single-fiber push-out, the influence of neighboring fibers and thermally induced residual stresses is shown. The interface damage initiates in the single-fiber push-out test at the indented fiber at positions closest to other fibers under the surface. In addition this is the position where the radially largest fiber expansion due to the Poisson effect is found. The results reveal that although the push-out test is simple to perform, the interpretation of its results might be a complicated task.

1. Introduction

Fiber reinforced polymers possess a high potential in lightweight constructions due to their low density and high strength and stiffness. Applications can be found in the automotive, aerospace and wind energy industries where the reduction of weight is essential in order to meet the present CO_2 reduction requirements. Fiber reinforced polymers are manufactured with continuous or discontinuous fiber reinforcement. Whereas classical unidirectional (UD) continuously fiber reinforced materials give the highest performance, discontinuous short or long fiber composites can be manufactured at much lower expenses and into complex structural components.

This paper focuses on the microstructure of a discontinuous glass-fiber reinforced sheet molding compound (SMC) with a thermoset matrix material consisting of an unsaturated polyester polyurethane hybrid resin (UPPH). The material is advantageous especially for automotive applications because of its mass-production compatibility. Due to the compression molding in the manufacturing process, the investigated material possesses a bundle-like microstructure, as can be seen in X-ray computed tomography investigations [1,2] or in micro-tensile tests [3]. The investigation and characterization of the fiber–matrix interface is important for the assessment of damage-initiation of the glass fiber reinforced SMC, as micro-tensile tests on this material [3] show crack initiation at the fiber–matrix interface. Crack propagation

inside a bundle, between bundles and in the matrix-rich regions occurs afterwards. Particularly for discontinuous reinforced polymers, the fiber–matrix interface is necessary for the load transfer from matrix to the fibers and back.

In literature, several methods have been established to characterize the fiber–matrix interface. In the fiber fragmentation test, one or several fibers are completely embedded in a matrix material and tension load is applied on the matrix. The breaking of the fiber into several parts is observed in combination with interface debonding and matrix cracks [4]. In the fiber pull-out test one fiber end is embedded in matrix material and pulled out to characterize the interface [5]. In the microbond test a droplet of matrix is pulled of the fiber [6]. All these tests have in common that their fiber–matrix interface is created under laboratory conditions and the determined interface parameters might be difficult to compare to the interface parameters of the composite under process conditions. For example the apparent interfacial shear strength of a microbond test can vary by more than a factor three depending on the atmospheric conditions during the preparation process [3]. The single-fiber push-in and push-out test are both used to investigate the interface behavior of the composite material. At the push-in test, a thicker specimen is polished on one side and load is applied on a fiber lying vertically to the surface by an indenter tip. The debonding of the

---

* Corresponding author at: Fraunhofer Institute for Mechanics of Materials IWM, Wöhlerstr. 11, 79108 Freiburg, Germany.
  E-mail address: benedikt.rohrmueller@iwm.fraunhofer.de (B. Rohrmüller).

fiber from the matrix material on the specimen surface, called push-in, can be observed. No information on the length of the crack can be determined. At the push-out test, a thin slice of material is polished on both sides with fibers vertical to the surface. The fibers are loaded axially by an indenter tip and interface debonding can be observed by a push-in of the fiber on the front side and a push-out of the fiber on the back side. The complete fiber–matrix debonding process can be observed. The radial fiber expansion due to its compression by the indenter tip might lead to an overestimation of the interface strength, as stated in [7]. The single-fiber push-out test goes back to the work of Marshall and Oliver [8,9] on ceramic-matrix composites. In [9] the cyclic push-out test was proposed to get an information on the debond fracture energy. This method was further developed by [10] to identify a value for the interface fracture toughness directly from experiments by an energy-based model. This method was extended and applied on polymer–matrix composites in [11–14].

Ref. [14] makes a distinction between abrupt and successive push-out behavior. In the abrupt push-out behavior, the interface crack propagation gets unstable after reaching the maximum force and the force flux abruptly drops. In the successive push-out behavior, a stable debonding occurs between fiber and matrix until complete debonding. Then friction between the debonded fiber and the surrounding matrix becomes the only dissipation mechanism, resulting in a plateau at the end of the force–displacement curve. For polymer–matrix composites both abrupt and successive push-out behavior can be found, also at different fibers on the same material [14]. Experimental single-fiber push-out tests can be used to test different interfaces and influence of fillers like nano-particles or carbon nano tubes [12,15].

Simulation models of single-fiber push-out [12,16,17] or push-in tests [18,19] often assume an isotropic linear elastic matrix behavior. However, an elasto-plastic matrix material model for an epoxy resin showed better agreement between experimental and numerical force–displacement curves than the linear elastic matrix material model [20, 21]. Because of the nonlinear elastic behavior of polymers, a nonlinear elastic Neo-Hooke model with a Prony series for time-dependent viscoelastic effects for the matrix model is employed in the present study. This matrix model is calibrated by simulations of experimental nanoindentation tests on matrix-rich regions of the composite.

The aim of this paper is to characterize a fiber–matrix interface model with a single-fiber push-out test through experiments and simulations. Nanoindentation is used to characterize the polymeric matrix material. Nanoindentation offers the possibility to investigate the matrix behavior directly on the composite on the microstructural level. Material model parameters that can be derived directly from experimental nanoindentation curves as described and established in [22,23] are the modulus and the hardness. A nonlinear viscoelastic material model is used to simulate the nanoindentation and modified to calibrate the simulated force–displacement curve to the experimental curves following [24,25].

2. Experimental investigation

2.1. Material

The investigated material is a glass fiber reinforced SMC. In its manufacturing process chopped fiber bundles with a length of about 25 mm are randomly distributed on the UPPH resin. These pre-impregnated fibers are then compression molded. Details on the manufacturing process can be found in [26]. In the present study, SMC sheets manufactured by Fraunhofer ICT were investigated. The manufacturing process leads to a microstructure where the fibers are arranged in fiber bundles with stochastic orientation. An exemplary micrograph with different fiber bundles is shown in Fig. 1. The fibers are grouped and form the bundle microstructure. Since the glass fibers are circular, fibers that appear as differently shaped ellipses in cross-section are oriented in
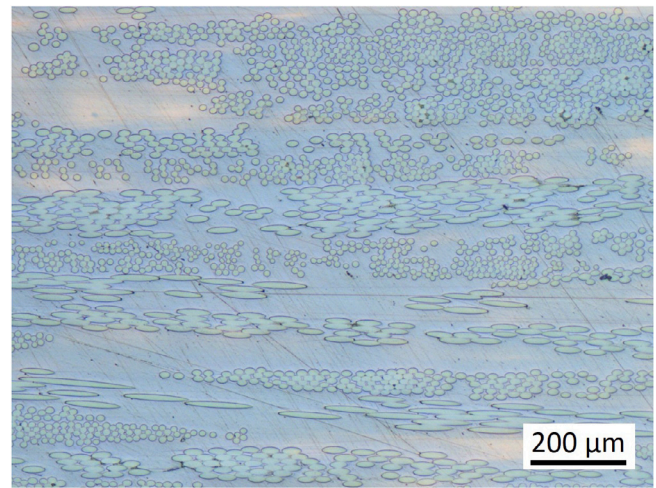

Fig. 1. Glass fiber SMC microstructure with fibers arranged in bundles.

different directions. Several fiber bundles are visible with matrix-rich regions in between.

The nanoindentation specimen was taken from the cross section of a material plate which was ground and polished to a thickness of about 1 mm. The specimen was not thinned further to avoid a large influence of the substrate on the measurement. The specimen was glued on a specimen holder for indentation testing.

To prepare the specimens for the push-out test, thin slices with a thickness of 1 mm were cut from the cross section of a material plate. The material slices were ground and polished from both sides to get a thickness of about 50 μm and a plane surface on both sides. The specimens were glued on a sample holder to reduce the compliance in the force–displacement curves for the push-out experiments and avoid bending of the specimens during testing. The sample holder consists of aluminum with grooves of 70 μm located under the indented fibers. The grooves in the sample holder were manufactured by micromilling.

2.2. Nanoindentation

The matrix behavior is investigated on the matrix-rich regions of the composite material, where the influence of neighboring fibers is assumed to be negligible. The nanoindentation experiments were carried out on a polished specimen with a Triboindenter TI-950 from Hysitron. For the testing a diamond Berkovich modified tip was used, formed by a three-sided pyramid with a half angle of 65.27°. For the loading part of the indentation curve, the ratio of the loading rate divided by the load $\dot{P}/P$ is held constant. Then the force is kept constant for 100 s to account for possible creep and relaxation effects. Indentation tests were performed for constant rates $\dot{P}/P$, of 2, 0.5, 0.1 and 0.01/s. For each $\dot{P}/P$ ratio, five tests were performed.

2.3. Single-fiber push-out test

A sketch of the single-fiber push-out test is shown in Fig. 2(a). The indenter tip is placed in the center above the fiber which shall be pushed out. This fiber should be located above the groove of the specimen holder.

The push-out tests were performed with the same Hysitron TI-950 Triboindenter as the indentation tests, however by using a different indenter tip. For the push-out tests, a diamond conical flat end indenter tip with a diameter of 5 μm and an angle of 60° was used. As the investigated glass fibers have a diameter of about 13 μm only the indented fiber is touched. For the positioning of the indenter tip above the fiber, the dual head option of the Triboindenter was used with
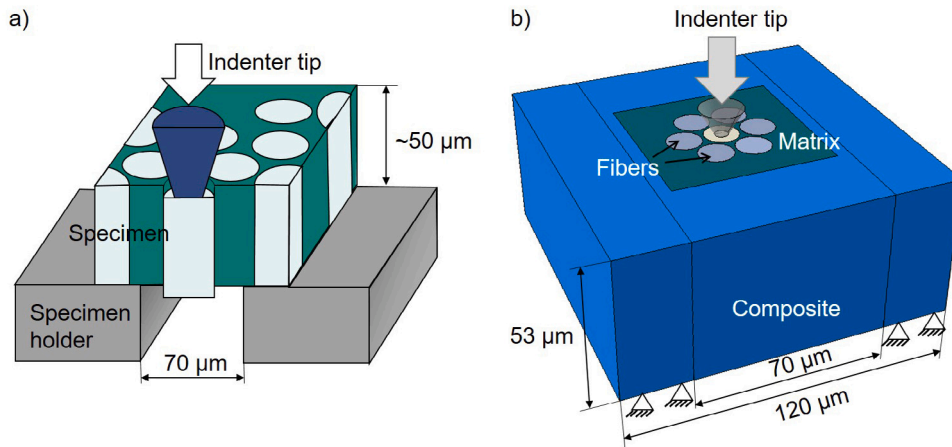
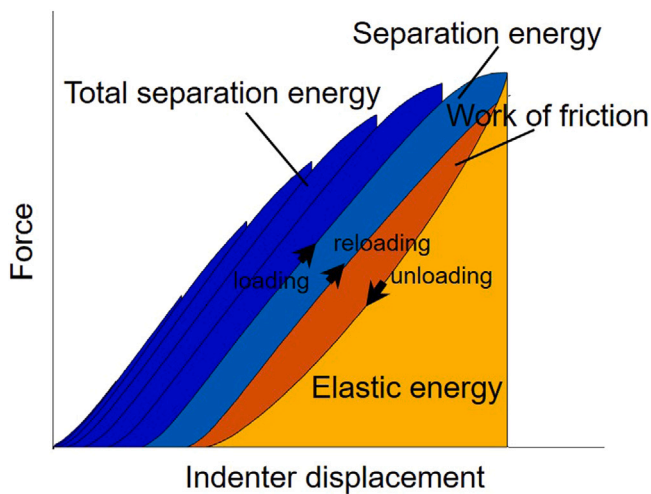**Fig. 2.** Push-out test: (a) experimental setup after [15] and (b) simulation model.

Fig. 3. Different energy contributions to a cyclic push-out test after [11].

a Berkovich modified tip for scanning. It works similar to an atomic force microscope. Only fibers perpendicular to the surface which show a circular contour on the surface were investigated. Among those, fibers with more than a slight indenter imprint were excluded from the evaluation. The tests were performed under displacement control with a displacement rate of 50 nm/s until an indenter displacement of 5 µm is reached. Additionally, cyclic tests were performed with loading and unloading cycles with increments of 200 nm per cycle. The cyclic push-out tests have the advantage that a value for the fracture toughness can be extracted directly from the experimental results. The method was developed in [10] and [27] for ceramic matrix composites and extended on carbon fiber reinforced polymer matrix composites in [11] and [21].

Using this method, cyclic single-fiber push-out tests are evaluated energetically, considering the areas under the force-indenter displacement record. According to [10,11] a selected loading–unloading and reloading cycle is separated in the elastic, friction and plastic/crack growing energy part. To avoid misunderstandings, the "plastic" energy is termed separation energy in the present paper, as it is the energy necessary for crack growth. An exemplary cyclic push-out curve with the different energy contributions is plotted in Fig. 3. The elastic energy is the area under the unloading curve. The friction work is the area between the unloading and reloading curve, the separation energy is given by the area between the loading and the following reloading curve, and the total separation energy is the accumulated separation energy which is the energy put into stable crack growth. Whereas for

most materials an unstable crack growth behavior in the single-fiber push-out test can be found in the literature, [28] and [14] found a stable crack growth until complete debonding on some polymer matrix composites. The fracture toughness then can be calculated by

$$fracture\ toughness = \frac{total\ separation\ energy}{cylindrical\ fiber\ surface\ area}. \tag{1}$$

Evaluating a push-out test only experimentally, the apparent interfacial shear strength (apparent IFSS) can be defined [10,15,29–31]:

$$\tau_{mean} = \frac{F_{\max}}{2\pi r_F l_F}, \tag{2}$$

where $F_{\max}$ is the maximum force, r_F the fiber radius and l_F the fiber length.

3. Simulation

The experiments are assessed further by means of a numerical simulation. In this context, finite element simulations of the nanoindentation are performed to characterize the matrix material. Simulations of the single-fiber push-out test are performed to characterize the interface. Abaqus/Standard is used for the nanoindentation simulations and Abaqus/Explicit for the push-out simulations.

3.1. Nanoindentation

For the modeling of the nanoindentation, a 60° model of the Berkovich modified tip and the underlying matrix material is used. Influences of tip rounding and surface roughness are neglected. Friction effects between indenter tip and specimen are not taken into account either, since investigations by [32] show that their influence in nanoindentation simulations is small. The indenter tip is modeled as a rigid body. The matrix is modeled by 3D linear hexahedral elements assuming a Neo-Hooke material model with a Prony series to model viscoelastic behavior.

The Neo-Hookean model's strain energy potential is given by

$$\Psi = C_{10}(\bar{I}_1 - 3) + \frac{1}{D_1}(J - 1)^2 \tag{3}$$

with $\bar{I}_1$ as the deviatoric strain invariant, J as the determinant of the deformation gradient and the material parameters C_{10} and D_1. To get a viscoelastic material response, a Prony series is used to describe the time dependence of the dimensionless shear modulus

$$g_R(t) = 1 - \sum_{i=1}^{N} g_i(1 - \exp(-t/\tau_i)) \tag{4}$$

Table 1
Material parameters of UPPH-matrix.

C_{10}^{∞} [MPa]	D_1 [1/MPa]	i [−]	g_i [−]	τ_i [s]
419	0.00148	1	0.134	1.84
		2	0.109	33.0
		3	0.0148	653

with the material parameters g_i and τ_i, the number of series parameters N and the time t. This leads to

$$C_{10}(t) = \frac{C_{10}^{\infty}}{1 - \sum_{i=1}^{N} g_i} g_R(t), \tag{5}$$

with the parameter C_{10}^{∞} describing the equilibrium curve after complete relaxation. The parameter D_1 and likewise the compressible part of the strain energy potential is assumed to be time independent, to reduce the number of parameters. For the parameter determination of the material model with $N = 3$, the simulation model is fitted to the loading and holding part of all experimental curves shown in Fig. 4(a). For the loading part the indenter tip is moved force controlled with the same $\dot{P}/P$ ratios as in the nanoindentation experiments in Section 2.2. The parameter determination is carried out using a generic algorithm in Python.

The resulting experimental nanoindentation curves are shown in Fig. 4. In (a) a single curve from the five recorded curves is shown for each rate. It was selected not to be at the extreme for any local rate but rather to represent a "monotone" behavior. These curves are taken for the parameter determination in the simulation. In (b) all curves for the highest and lowest rate are shown.

Each curve can be separated into three parts: (i) the loading part, starting from zero displacement, (ii) the holding part, where the force is held constant and creep takes place and (iii) the unloading part, where the force goes down again. Viscoelastic effects can be observed for the different rates because on the loading part of the curves for a higher rate a higher force is needed at the same displacement. Additionally, the curves with higher rate during the loading exhibit a larger amount of creep deformation during the holding time. As a consequence, the unloading curves for the different rates are more or less equal. The parameters of the Neo-Hooke model and the Prony parameters were adapted to the loading and holding part of all four nanoindentation curves shown in Fig. 4(a). The fitting was performed in the time domain. The resulting curves are shown in Fig. 5 and the resulting parameters for the matrix material in Table 1. The nanoindentation simulation curves are in a rather good agreement with their experimental counterparts, giving evidence for the adequacy of the chosen material model.

3.2. Single-fiber push-out test

The simulation model of the push-out test is shown in Fig. 2(b). The indented fiber is positioned in the center and surrounded by neighboring fibers and matrix. Only the inner range is modeled in a detailed manner with explicit modeling of the fibers and the matrix by using 3D linear hexahedral elements with reduced integration and an edge length of 1 μm. In parametric studies with different mesh densities, the simulation model was found to converge at this element size. The influence of more distant fibers and matrix is included by a surrounding area consisting of a transversally isotropic composite material. The five transversal isotropic composite parameters ($E_{\parallel} = 49.4\,\text{GPa}$, $E_{\perp} = 13.5\,\text{GPa}$, $\nu = 0.27$, $G_{\parallel} = 10.0\,\text{GPa}$, $G_{\perp} = 9.1\,\text{GPa}$) are determined by a Mori–Tanaka homogenization implementation [33]. The local fiber volume content inside the fiber bundle (66%) is used as the prescribed volume fraction for the composite of the FE model. The isotropic linear elastic UPPH neat matrix parameters for the homogenization are taken from [34] and shown in Table 2 together with the linear elastic glass

Table 2
Material parameters.

Parameter	Symbol	Value	Unit
Young's modulus glass fibers	E_F	73	GPa
Poisson's ratio glass fibers	ν_F	0.22	–
Young's modulus UPPH [34]	E_M	3.4	GPa
Poisson's ratio UPPH [34]	ν_M	0.385	–
Thermal expansion coefficient UPPH [34]	α_M	7.45e−5	1/K
Thermal expansion coefficient glass fibers	α_F	5e−6	1/K

fiber parameters. Boundary conditions are applied to the composite block according to the experiment, as can be seen in Fig. 2(b). The outer blocks are clamped on the bottom side.

The fiber–matrix interface is modeled by a cohesive zone model. The interface stresses in the normal and the two shear directions t_n, t_s and t_t are in this case connected to the relative displacements δ_n, δ_s and δ_t in the same directions by an uncoupled traction separation law

$$\begin{Bmatrix} t_n \\ t_s \\ t_t \end{Bmatrix} = \begin{bmatrix} K_{nn} & & \\ & K_{ss} & \\ & & K_{tt} \end{bmatrix} \begin{Bmatrix} \delta_n \\ \delta_s \\ \delta_t \end{Bmatrix} \tag{6}$$

with the initial stiffnesses K_{nn}, K_{ss} and K_{tt} in the normal and the two shear directions. In general K is seen as a numerical parameter which has to be chosen large enough. As later described in the result section the slope in the numerical force–displacement curve of a push-out test can be influenced by its size as well, thus modeling a compliant interface. The interface damage initiation is modeled by a quadratic stress criterion

$$\left\{ \frac{\langle t_n \rangle}{t_n^c} \right\}^2 + \left\{ \frac{t_s}{t_s^c} \right\}^2 + \left\{ \frac{t_t}{t_t^c} \right\}^2 = 1 \tag{7}$$

with t_n^c, t_s^c and t_t^c as the critical traction in normal and the two shear directions, respectively. As the critical interface strength is not directly comparable to the interfacial shear strength from Eq. (2), the critical traction is adapted directly to the experimental push-out curves. To compare to the fracture toughness values from the experimental cyclic push-out tests, the damage evolution is modeled based on an energy criterion. It is described by the following form

$$\left\{ \frac{\mathcal{G}_n}{\mathcal{G}_n^c} \right\} + \left\{ \frac{\mathcal{G}_s}{\mathcal{G}_s^c} \right\} + \left\{ \frac{\mathcal{G}_t}{\mathcal{G}_t^c} \right\} = 1 \tag{8}$$

with the critical fracture toughness $\mathcal{G}_n^c$, $\mathcal{G}_s^c$ and $\mathcal{G}_t^c$ in the normal and the two shear directions. For the completely debonded fiber–matrix interface Coulomb friction with a friction coefficient μ is assumed. Thermal stresses are added to the model as a predefined field from a load free implicit cooling step. The model is therefor assumed to be stress-free at the manufacturing temperature of 145 °C and cooled down to ambient temperature. The necessary thermal expansion coefficients are given in Table 2.

4. Results

4.1. Push-out test results

The experimental push-out curves for a selected fiber bundle are presented in Fig. 6. The force divided by the fiber surface area is plotted on the ordinate, to exclude effects of different fiber diameters. The behavior of the push-out curves can be summarized as follows: After a shallow increase of the force in the beginning, the force increases linearly when full contact between indenter tip and fiber is established. Then the force-indenter displacement curve becomes nonlinear before the maximum is reached. The force then decreases until complete debonding. The push-out behavior is successive (not instantaneous) with a stable crack growth. Sometimes the push-out behavior is accompanied by a drop in force. It remains unstable only for a short
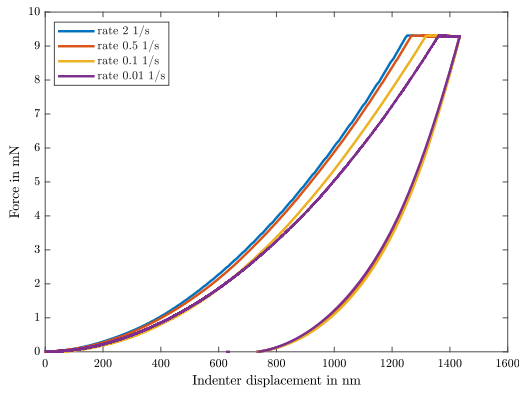
(a) One exemplary curve per $\dot{P}/P$ ratio.
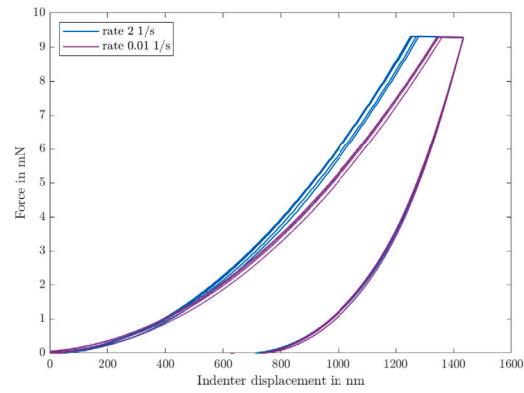
(b) All curves for highest and lowest rate.

Fig. 4. Experimental nanoindentation curves with different rates for the loading part. (For interpretation of the references to color in this figure legend, the reader is referred to the web version of this article.)
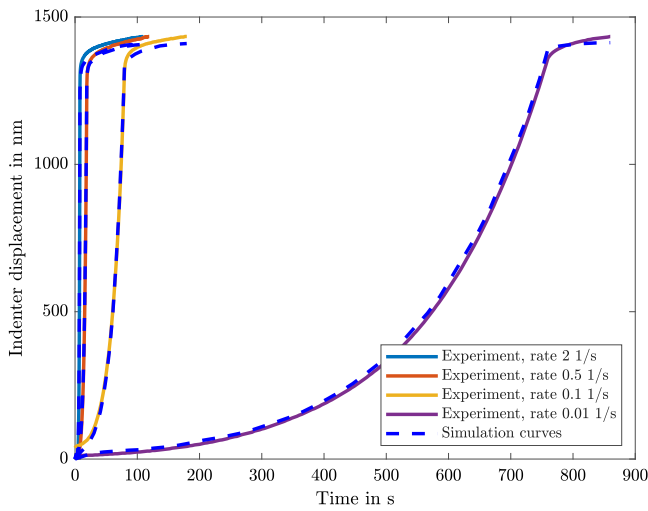

Fig. 5. Nanoindentation simulation curves adapted on loading and holding part of experimental curves in the indenter displacement time domain. The experimental curves are taken from Fig. 4(a) with decreasing rate from left to right.
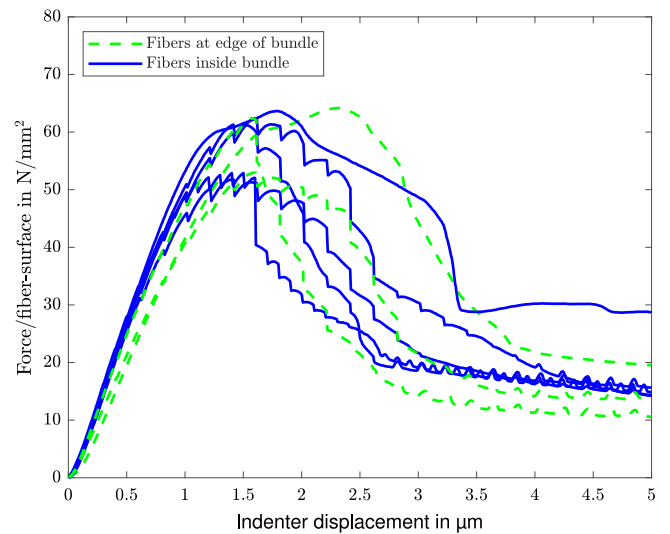

Fig. 6. Experimental push-out curves on one fiber bundle. For cyclic tests only the enveloping curve is plotted.

crack part and then becomes stable again. On the plateau at the end of the curves friction is the only dissipating mechanism between fiber and matrix. From the cyclic push-out tests only the enveloping curves are shown in order not to overload the graph. This explains the non smooth behavior of some curves. For fibers at the edge of a fiber bundle which are surrounded only on one side by other fibers, the slope of the force–displacement curve is lower. This effect was also observed at other fiber bundles. Regarding the apparent interfacial shear strength from Eq. (2), which is the maximum of every curve in Fig. 6, the fibers can be divided into two groups based on its apparent interfacial shear strength: one group of fibers with an apparent interfacial shear strength of about 65 MPa and another group with an apparent interfacial shear strength of about 50 MPa. The differences seem to be independent of the position of the fiber in the bundle.

Fig. 7 shows the force–displacement curve of a typical cyclic push-out curve. Successive push-out behavior can be clearly observed. The corresponding SEM-images after testing show a fiber inside a fiber bundle which is pushed-in on the front and pushed-out on the back side. The energy contributions in Fig. 8 are evaluated as described in Section 2.3. They show the elastic, friction, separation and total separation energy contributions for the single cycles. The total separation energy, which is the accumulated separation energy up to this cycle, is increasing almost linearly between 1 and 3 µm indenter displacement. These two points – the start and end of the linear increase of the accumulated separation energy – are identified after [11,14] as the push-in and push-out of the indented fiber. The push-in and push-out are also plotted as dashed lines in the force–displacement curve in
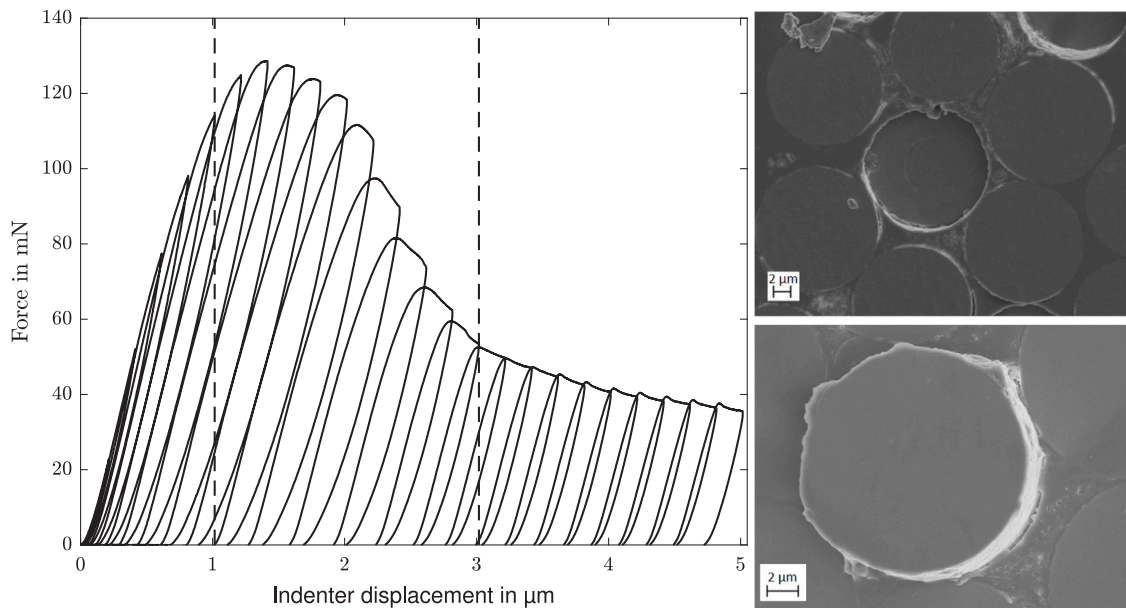
Table 3
Determined interface parameters.

Interface parameters	Friction coefficient	Critical fracture toughness	Initial stiffness	Critical traction	Apparent interfacial shear strength from Eq. (2)
	μ	$\mathcal{G}^c_{n,s,t}$	$K_{nn,ss,tt}$	$t^c_{n,s,t}$	τ_{mean}
Unit	[−]	[J/m²]	[N/mm³]	[MPa]	[MPa]
Fiber inside bundle	0.35	107	10^7	70	64.2
Fiber outside bundle	0.35	107	10^7	70	63.7
Fiber with weaker interface	0.35	81.3	10^6	57	52.9

Fig. 7. Cyclic push-out curve with indented fiber after test from front and back side of the specimen.
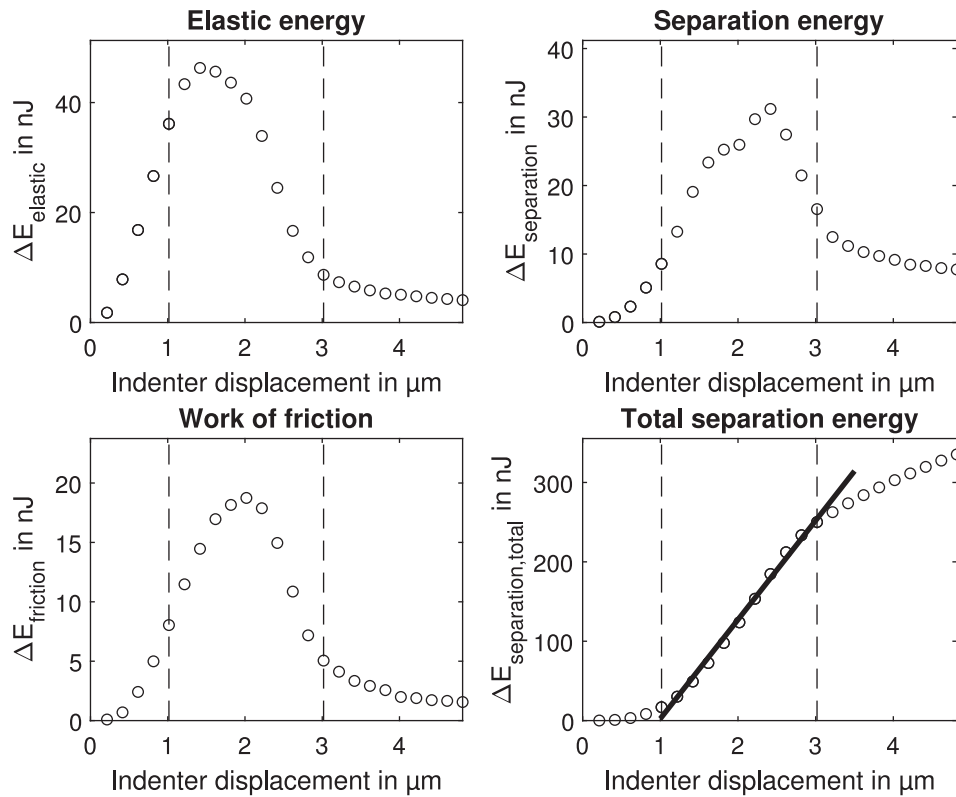

Fig. 8. Different energy contributions for each cycle of push-out test plotted over indenter displacement. Dashed lines are push-in of the fiber on the front side and push-out on the back side of the specimen.

Fig. 7. This shows that the fiber is pushed-in on the front surface before the maximum force is reached. Averaging over 13 cyclic push-out tests results in an experimental fracture toughness of $107 \pm 20 \, \text{J/m}^2$.

4.2. Push-out simulation results

Fig. 9(a) shows simulation and experimental push-out curves of three different microstructures: one fiber inside a fiber bundle, one fiber at the edge of a fiber bundle and one fiber inside a fiber bundle

with a lower maximum force. The geometry of the simulation model was as shown in Fig. 2(b) with the three different microstructures from Fig. 9(b)–(d) in the inner region. The simulation curves can be adapted to the experimental curves by tuning the interface parameters. As there is only one type of experiment, no distinction is made between the different modes of crack growth and the interface parameters for the normal and the two shear directions are set to the same value. The remaining four interface parameters – the critical fracture toughness, the initial stiffness, the critical traction and the friction coefficient
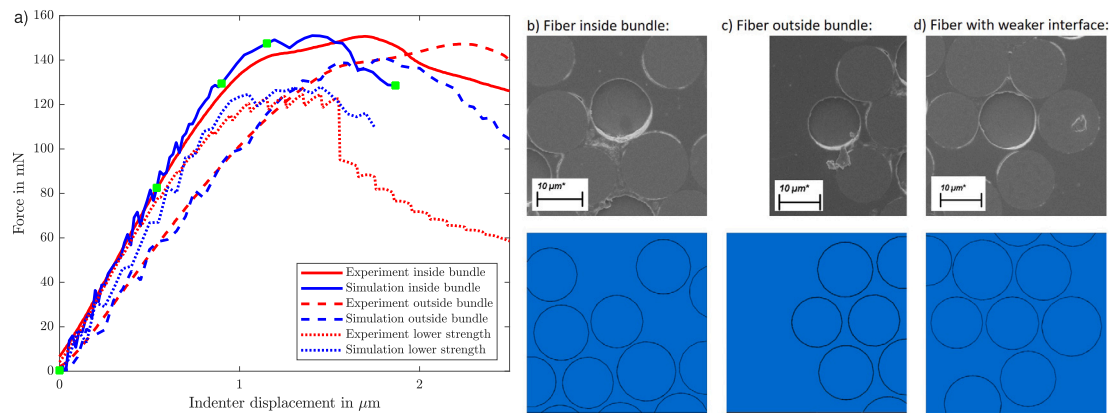
Fig. 9. Push-out curves of three experiments and simulations with corresponding microstructure: (a) force indenter displacement curves with experimental microstructure (always top) after test and simulation microstructure (bottom) of (b) fiber inside fiber bundle, green dots are interface damage evolution from Fig. 10, (c) fiber outside fiber bundle and (d) fiber with weaker interface with indented fiber in the middle. The interface damage for the green dots on the simulation curve inside the fiber bundle is shown in Fig. 10. (For interpretation of the references to color in this figure legend, the reader is referred to the web version of this article.)
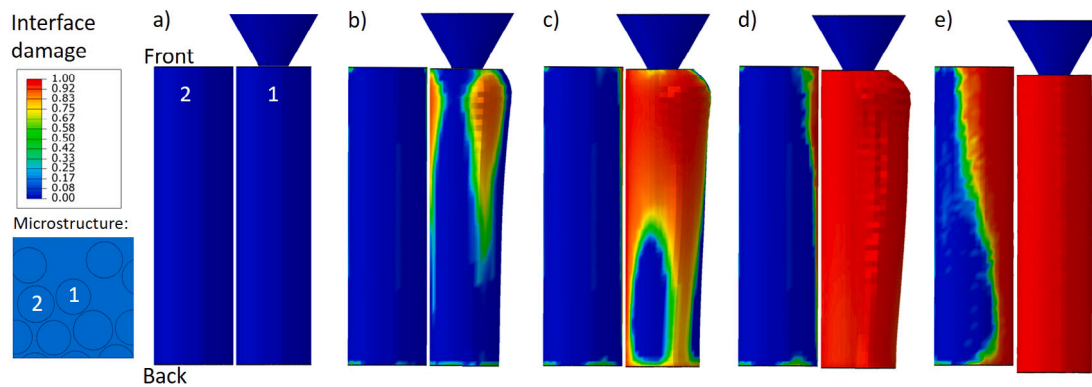

Fig. 10. Interface damage evolution of simulation of fiber inside fiber bundle from Fig. 9(b) at displacements of 0, 0.54, 0.90, 1.15 and 1.87 μm. The corresponding points are marked with green dots in the force indenter displacement diagram in Fig. 9(a). Depicted is the indented fiber with the neighboring fiber on the left. In (b)–(d) the right side of the indented fiber is scaled radially by a factor of 50 to show the radial expansion during testing. (For interpretation of the references to color in this figure legend, the reader is referred to the web version of this article.)

– are given in Table 3. However, in the simulation, the interface reaches a completely damaged state somewhat earlier i.e. at a lower indenter displacement and then terminates. The differences between the two curves of the fiber inside and outside the bundle is only due to the geometry. Only for the fiber with weaker interface, the interface parameters are different: the initial stiffness, the critical traction and the critical fracture toughness are all smaller. The critical fracture toughness of the fiber with weaker interface is directly taken from the experimental measurement of this fiber since it is the enveloping curve of a cyclic push-out curve.

In addition to the critical traction of the interface model from the simulation, the experimentally determined interfacial shear strength determined from Eq. (2) is given (see Table 3). The interfacial shear strength is lower than the critical traction in all three cases.

The interface damage evolution on the indented fiber and one neighboring fiber are shown in Fig. 10 at five different times for a fiber inside a fiber bundle. The corresponding instants in time are marked with green dots in the force–displacement diagram in Fig. 9(a). The interface damage initiates at the upper part of the indented fiber at positions near to other fibers. Somewhat below the surface the fiber expands laterally under compression by the indenter tip due to the Poisson effect. Contrary on the surface itself, the elastic imprint of the indenter leads to tensile normal stresses on the fiber–matrix interface. The radial fiber expansion is made visible by scaling the radial displacement of the indented fiber (only on the right) in Fig. 10(b)–(d) by a factor of 50.

After the interface at the indented fiber has almost completely failed, an increasing damage of the interface at the neighboring fiber can be observed in Fig. 10 (and all other neighboring fibers).

For a deeper insight into the debonding process, the separation between fiber and matrix is investigated in more detail. In order to also account for the effect of residual stresses, two competitive simulations with and without thermally induced residual stresses are performed. The thermally induced residual stresses are included by assuming a stress-free temperature in the range of the manufacturing temperature (here 145 °C) and performing a load-free cooling step to ambient temperature before the push-out simulation as described in Section 3.2. Fig. 11(a) shows the simulation results for the fiber inside the fiber bundle of the microstructure from Fig. 9(b) with and without thermally induced residual stresses. Adding residual stresses results in an increased force for indenter displacements larger than 1.2 μm. In addition to the force–displacement curve, the axial separation of the indented fiber from the surrounding matrix (mean nodal displacement) is plotted for the front and back side of the specimen. The explanation of front and back side is given in Fig. 10(a). The interface debonding process appears to be dominated for both simulation cases by the separation on the front side at displacements larger than 1 μm. However, the separations for the simulation with residual stresses are delayed. The thermally induced residual stresses lead to an axial mismatch between indented fiber and surrounding matrix in the simulation model at the beginning since the simulation model is assumed flat before cooling and
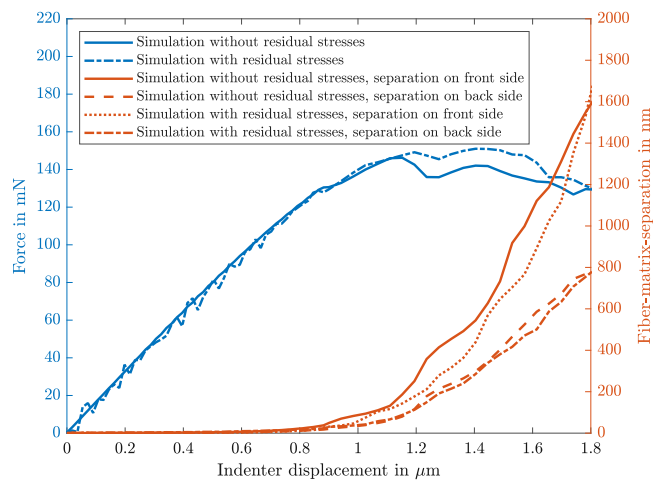
Fig. 11. Simulation results of fiber inside fiber bundle from Fig. 9(b) with and without thermally induced residual stresses. For explanation of meaning of front and back side refer to Fig. 10.

since the matrix has a higher thermal expansion coefficient than the fibers. Consequently the fibers are radially compressed but stand out axially of the matrix material on both specimen sides at the beginning of the simulation.

5. Discussion

We first focus on the accuracy of the material data of the determined UPPH matrix material. The experimental nanoindentation curves clearly show a viscoelastic behavior with higher forces for higher loading rates at the same displacement. The experimental curves of the same rate (Fig. 4(b)) show only little scatter. Differences could be caused by variations in the surface roughness, local varying material behavior or a drift in the piezo actuator of the indenter tip especially for lower rates. The surface roughness and adhesive effects between indenter tip and specimen surface in the experiment might lead to a slightly underestimated numerical stiffness of the matrix material. Further differences between experimental and simulated nanoindentation are due to a slight rounding of the indenter tip and possible adhesive effects or a remaining surface roughness, which are not considered in the simulation. For the obtained viscoelastic material parameters all these remaining inconsistencies between model and experiment are regarded as minor since the viscoelastic model is able to nicely reproduce the experimental indentation curves for all the different loading rates (Fig. 5).

In the present investigation, the nanoindentation specimen was taken from the "real" composite material and not from bulk material. The advantage of this approach is, that the material is investigated under the same manufacturing conditions as for the matrix in the push-out test. Thus, the results are representative for the material in-situ, i.e. in the state after polymerization in the composite material. Thus, the proposed material characterization by nanoindentation provides a high-precision tool for determination of the matrix material parameters of composites in the relevant state. It should be mentioned that the polymerization state and thus the mechanical properties of the matrix may differ between positions inside fiber bundles and matrix-rich regions outside fiber bundles. However, indentation measurements inside fiber bundles are again influenced by the stiff fibers and are difficult to perform as there are some slight differences in height between fibers and matrix caused by different removal rates in the preparation process.

Concerning the push-out tests, the slope of the single-fiber push-out tests in Fig. 6 appears to be dominated by the position of a fiber inside a fiber bundle or more generally by the stiffness of the surrounding

material. This is also confirmed in the push-out simulations in Fig. 9 (a), where the variation in the curves of the fibers inside and outside the bundle are caused just by the different geometries.

The weaker interface of some fibers could be due to the scatter of the material parameters from the manufacturing process. However, it also cannot be excluded that its interface might have been damaged during sample preparation or push-out tests of other fibers on the sample.

While the apparent interfacial shear strength from Eq. (2) is a "global" value for the entire experiment, the cohesive zone critical interface traction is a local value which needs to be overcome to enable interface damage. Thus, it is clear that the two values are not directly comparable and it also means that an interfacial shear strength determined experimentally by a push-out test cannot be directly used in a simulation model.

The friction part of the push-out curves in Fig. 6, the amount of force after complete debonding, when the force is more or less constant, varies between different fibers. This may be due to different surface roughnesses of the different fibers, or due to different residual stresses on different fibers, or due to a slightly imperfect debonding of the fiber–matrix interface. Residual stresses are induced due to the difference in the coefficients of thermal expansion of fibers and matrix in conjunction with the elevated manufacturing temperature. Especially for the fibers at the edge of a fiber bundle, the deviation in the friction part is larger.

In the separation energy plot of the cyclic push-out test in Fig. 8 top right a slight increase of energy in two cycles before the energy per cycle drops down toward the push-out can be observed. This effect of increased separation energy before the fiber push-out in this evaluation method can also be observed in diagrams in [14]. Due to the Poisson effect, the fiber, which is axially loaded by the indenter tip, expands radially in the upper part, as observed in the present simulation. This effect results in an additional pressure between fiber and matrix which has to be overcome to provoke crack growth. In contrast, in the lower part of the fiber a lower crack growth resistance exists which results in an increased crack growth energy per cycle (for cycles with constant displacement increments). The increased separation energy with an energy of about $30\,\mathrm{nJ}$ per cycle in the second part of the push-out test in Fig. 8 top right could be interpreted as this increased crack growth velocity in the second part of the push-out process.

The push-out simulations reveal a strong interaction between neighboring fibers. Since the simulations show that interface damage in the push-out process also occurs at neighboring fibers, which is not taken into account in the experimental evaluation, the experimentally determined fracture toughness according to the standard evaluation overestimates the real value. However, as the simulation curves fit quite well to the experimental curves, an overestimated fracture toughness might be compensated in the present investigation by underestimated residual stresses, as residual stresses additional to the thermally induced ones are not considered.

The push-out simulations show that the interface damage initiates at the interface of the indented fiber nearby the surface where fibers are close together. Similar observations were made in [21] where it was also found that the interface damage initiation in push-out simulations starts in areas where fibers are close together. In the current investigation this is the location where the largest radial expansion of the fiber is obtained during testing. That radial expansion of the indented fiber occurs due to its compression by the indenter tip, has been described by [7].

The influence of thermally induced residual stresses plays an important role in the simulation results. As the matrix material features a higher coefficient of thermal expansion than the fibers, a pronounced radial pressure from the matrix onto the fibers and subsequently a pronounced frictional force develop. This effect is represented in the force-indenter displacement diagram through an increased force after the interface is already partly damaged. The influence of additional residual stresses like curing residual stresses should be considered

further since by this means, the residual stresses might be covered in an improved manner.

The single-fiber push-out test gives the possibility for an in-situ investigation of the fiber–matrix interface on the composite material with a predefined location of crack initiation and direction of crack propagation. The problems of specially prepared specimens as in other single fiber tests (microbond test, pull-out test, fiber fragmentation test etc.), all featuring a specially prepared matrix and thus possibly non-representative interface properties are avoided since specimens can be prepared directly from a piece of material taken from the actual manufacturing process. However, the interface damage at neighboring fibers should not be ignored in the evaluation as numerical simulations show.

6. Conclusion

The present contribution has been concerned with an improved determination of fiber–matrix interface properties for an SMC composite using single-fiber push-out tests in conjunction with numerical simulation of the experiments. Both, the influence of the neighboring fibers and the development of thermally induced residual stresses were investigated.

The matrix material, playing an important role in polymer–matrix composites, was characterized by nanoindentation directly on the composite. It is modeled nonlinear viscoelastic. With the chosen matrix material model, calibrated by nanoindentation experiments and simulations, and the cohesive zone model, the experimental curves could be reproduced up to the maximum strength.

The determined parameters can be further used for microstructure simulations and for investigations of the fiber–matrix adhesion. This is especially important for short fiber reinforced composites, where in comparison to UD material much more force transmissions from matrix onto fibers takes place. Therefore, and since the fiber direction is not aligned with the main loading direction, the fiber–matrix interfaces for chopped fiber composites are of crucial importance for the integrity of the material.

CRediT authorship contribution statement

Benedikt Rohrmüller: Conceptualization, Methodology, Investigation, Writing - original draft, Visualization, Project administration. **Peter Gumbsch:** Conceptualization, Resources, Writing - review & editing, Supervision, Funding acquisition. **Jörg Hohe:** Conceptualization, Resources, Writing - review & editing, Supervision, Funding acquisition.

Declaration of competing interest

The authors declare that they have no known competing financial interests or personal relationships that could have appeared to influence the work reported in this paper.

Data availability

The raw/processed data required to reproduce these findings cannot be shared at this time as the data also forms part of an ongoing study.

Acknowledgment

References

[1] Pinter P. Microstructure characterization of continuous-discontinuous fibre reinforced polymers based on volumetric images (Ph.D. thesis), Karlsruhe: Karlsruhe Institute of Technology; 2018, http://dx.doi.org/10.5445/IR/1000084499.

[2] Schöttl L, Weidenmann KA, Sabiston T, Inal K, Elsner P. Fiber bundle tracking method to analyze sheet molding compound microstructure based on computed tomography images. NDT E Int 2021;117:1–12. http://dx.doi.org/10.1016/j.ndteint.2020.102370.

[3] Schober M. On the characterization and modeling of interfaces in fiber reinforced polymer structures (Ph.D. thesis), Karlsruhe: Karlsruhe Institute of Technology; 2019, http://dx.doi.org/10.5445/IR/1000100455.

[4] Kelly A, Tyson WR. Tensile properties of fibre-reinforced metals: Copper/tungsten and copper/molybdenum. J Mech Phys Solids 1965;13(6):329–50. http://dx.doi.org/10.1016/0022-5096(65)90035-9.

[5] DiFrancia C, Ward TC, Claus RO. The single-fibre pull-out test. 1: Review and interpretation. Composites A 1996;27(8):597–612. http://dx.doi.org/10.1016/1359-835X(95)00069-E.

[6] Miller B, Muri P, Rebenfeld L. A microbond method for determination of the shear strength of a fiber/resin interface. Compos Sci Technol 1987;28(1):17–32. http://dx.doi.org/10.1016/0266-3538(87)90059-5.

[7] Piggott MR. Why interface testing by single-fibre methods can be misleading. Compos Sci Technol 1997;57(8):965–74. http://dx.doi.org/10.1016/S0266-3538(97)00036-5.

[8] Marshall DB. An indentation method for measuring matrix-fiber frictional stresses in ceramic composites. J Am Ceram Soc 1984;67(12):C–259–C–260. http://dx.doi.org/10.1111/j.1151-2916.1984.tb19690.x.

[9] Marshall DB, Oliver WC. Measurement of interfacial mechanical properties in fiber-reinforced ceramic composites. J Am Ceram Soc 1987;70(8):542–8. http://dx.doi.org/10.1111/j.1151-2916.1987.tb05702.x.

[10] Mueller WM, Moosburger-Will J, Sause M, Horn S. Microscopic analysis of single-fiber push-out tests on ceramic matrix composites performed with berkovich and flat-end indenter and evaluation of interfacial fracture toughness. J Eur Ceram Soc 2013;33(2):441–51. http://dx.doi.org/10.1016/j.jeurceramsoc.2012.09.009.

[11] Greisel M, Jäger J, Moosburger-Will J, Sause M, Mueller WM, Horn S. Influence of residual thermal stress in carbon fiber-reinforced thermoplastic composites on interfacial fracture toughness evaluated by cyclic single-fiber push-out tests. Composites A 2014;66:117–27. http://dx.doi.org/10.1016/j.compositesa.2014.07.010.

[12] Battisti A, Esqué-de los Ojos D, Ghisleni R, Brunner AJ. Single fiber push-out characterization of interfacial properties of hierarchical CNT-carbon fiber composites prepared by electrophoretic deposition. Compos Sci Technol 2014;95:121–7. http://dx.doi.org/10.1016/j.compscitech.2014.02.017.

[13] Kavouras P, Dragatogiannis DA, Batsouli DI, Charitidis CA. Effect of local microstructure on the indentation induced damage of a fiber reinforced composite. Polym Test 2017;61:197–204. http://dx.doi.org/10.1016/j.polymertesting.2017.05.023.

[14] Moosburger-Will J, Greisel M, Schulz M, Löffler M, Mueller WM, Horn S. Investigation of the fiber-matrix interaction in carbon fiber-reinforced polyether ether ketone by cyclic single fiber push-out and push-back tests. Compos Interfaces 2020;27(2):227–47. http://dx.doi.org/10.1080/09276440.2019.1620542.

[15] Godara A, Gorbatikh L, Kalinka G, Warrier A, Rochez O, Mezzo L, Luizi F, van Vuure AW, Lomov SV, Verpoest I. Interfacial shear strength of a glass fiber/epoxy bonding in composites modified with carbon nanotubes. Compos Sci Technol 2010;70(9):1346–52. http://dx.doi.org/10.1016/j.compscitech.2010.04.010.

[16] Fliegener S. Micromechanical finite element modeling of long fiber reinforced thermoplastics. Fraunhofer iwm forschungsberichte, Vol. 8, Stuttgart: Fraunhofer IRB Verlag; 2016.

[17] Brylka B, Fritzen F, Böhlke T, Weidenmann KA. Influence of micro-structure on fibre push-out tests. PAMM 2011;11(1):141–2. http://dx.doi.org/10.1002/pamm.201110062.

[18] Rodríguez M, Molina-Aldareguía JM, González C, LLorca J. A methodology to measure the interface shear strength by means of the fiber push-in test. Compos Sci Technol 2012;72(15):1924–32. http://dx.doi.org/10.1016/j.compscitech.2012.08.011.

[19] Wang J, Feng Y, Zhao G, Yang L, Xu J. Effect of elastic and thermal mismatch on push-in mechanism and shear strength measurement of fiber/matrix interface. Compos Interfaces 2020;27(10):921–35. http://dx.doi.org/10.1080/09276440.2020.1712917.

[20] Jäger J. Aspekte der Faser-Matrix-Wechselwirkung in carbonfaserverstärkten Polymeren. 1st ed.. Berlin: Mensch und Buch Verlag; 2014.

[21] Jäger J, Sause M, Burkert F, Moosburger-Will J, Greisel M, Horn S. Influence of plastic deformation on single-fiber push-out tests of carbon fiber reinforced epoxy resin. Composites A 2015;71:157–67. http://dx.doi.org/10.1016/j.compositesa.2015.01.011.

[22] Oliver WC, Pharr GM. An improved technique for determining hardness and elastic modulus using load and displacement sensing indentation experiments. J Mater Res 1992;7(6):1564–83. http://dx.doi.org/10.1557/JMR.1992.1564.

[23] Oliver WC, Pharr GM. Measurement of hardness and elastic modulus by instrumented indentation: Advances in understanding and refinements to methodology. J Mater Res 2004;19(1):3–20. http://dx.doi.org/10.1557/jmr.2004.19.1.3.

[24] Chen Z, Diebels S. Indentation of PU at different scales and computational modeling: identification of viscoelasticity and quantification of adhesion effects. Arch Appl Mech 2015;85(9–10):1225–43. http://dx.doi.org/10.1007/s00419-015-1008-5.

[25] Larsson P-L, Giannakopoulos AE, Söderlund E, Rowcliffe DJ, Vestergaard R. Analysis of berkovich indentation. Int J Solids Struct 1996;33(2):221–48. http://dx.doi.org/10.1016/0020-7683(95)00033-7.

[26] Böhlke T, Henning F, Hrymak AN, Kärger L, Weidenmann K, Wood JT, editors. Continuous–discontinuous fiber-reinforced polymers: An integrated engineering approach. Cincinnati, Ohio: Hanser Publications; 2019.

[27] Mueller WM, Moosburger-Will J, Sause M, Greisel M, Horn S. Quantification of crack area in ceramic matrix composites at single-fiber push-out testing and influence of pyrocarbon fiber coating thickness on interfacial fracture toughness. J Eur Ceram Soc 2015;35(11):2981–9. http://dx.doi.org/10.1016/j.jeurceramsoc.2015.04.033.

[28] Greisel M. Faser-Matrix-Anbindung in carbonfaserverstärkten thermoplastischen Polymeren (Ph.D. thesis), Augsburg: Universität Augsburg; 2017.

[29] Watanabe K, Kohyama A, Sato S, Serizawa H, Tsunakawa H, Hamada K, Kishi T. Evaluation of interfacial shear strength of c/c composites by means of micro-indentation test. Mater Trans JIM 1996;37(5):1161–5. http://dx.doi.org/10.2320/matertrans1989.37.1161.

[30] Chandra N, Ghonem H. Interfacial mechanics of push-out tests: theory and experiments. Composites A 2001;32(3–4):575–84. http://dx.doi.org/10.1016/S1359-835X(00)00051-8.

[31] Sha JJ, Dai JX, Li J, Wei ZQ, Hausherr J-M, Krenkel W. Measurement and analysis of fiber-matrix interface strength of carbon fiber-reinforced phenolic resin matrix composites. J Compos Mater 2014;48(11):1303–11. http://dx.doi.org/10.1177/0021998313485264.

[32] Hardiman M. Nanoindention characterisation of carbon fibre reinforced plastic microstructures (Ph.D. thesis), Limerick: University of Limerick; 2016.

[33] Bauer J. Meanfield-homogenization, v0.0.2. 2019, https://git.scc.kit.edu/julianbauerirtg2078/meanfield-lite/ (Accessed: 2020-08-24).

[34] Kehrer ML. Thermomechanical mean-field modeling and experimental characterization of long fiber-reinforced sheet molding compound composites (Ph.D. thesis), Karlsruhe: Karlsruhe Institute of Technology; 2019, http://dx.doi.org/10.5445/KSP/1000093328.